J. Materials, Conc. Struct., Pavements, JSCE, No. 599/V-40, 177-184, 1998 August

DAMAGE EVOLUTION BY ACOUSTIC EMISSION IN THE FRACTURE PROCESS ZONE OF CONCRETE

Masayasu OHTSU[1] and Masanobu OHTSUKA[2]

[1] Member of JSCE, Dr. of Eng., Professor, Dept. of Civil Eng. and Architecture, Kumamoto University
(Kurokami 2-39-1, Kumamoto 860, Japan)
2 Member of JSCE, Fukuoka Branch, Oriental Construction Corp.
(Tenjin 4-2-31, Chuou-ku, Fukuoka 810, Japan)

The moment tensor analysis of acoustic emission (AE) is reviewed, on the basis of the damage mechanics. The relation between the damage variable and the moment tensor is clarified. In bending tests of notched beams, the crack kinematics are determined. Tensile cracks are nucleated extensively at the outer region of the fracture process zone, while shear cracks are observed inside the zone and close to the final crack surface. The damage evolution process under the nucleation of the fracture process zone is estimated. It is found that the evolution process in cementitious materials is not necessarily dependent on the modes of final cracks, but associated substantially with the mechanisms of microcracking.

Key Words : acoustic emission, moment tensor analysis, fracture process zone, damage mechanics

1. INTRODUCTION

Acoustic emission (AE) method is an inspection technique to detect elastic waves generated in a material. In concrete, it was confirmed that AE waves due to cracking could be synthesized by the dislocation model[1]. The dislocation (crack) motion consists of kinetics and kinematics. In the source characterization of AE, crack kinetics is represented by a source-time function which can be determined by the deconvolution analysis[2]. Crack kinematics at AE source is defined by the crack motion vector (Burgers vector) and the unit vector normal to the crack plane. Combining with the elastic constants, the product of the two vectors leads to the moment tensor. A simplified and stable procedure was developed to determine the moment tensor components from AE waveforms[3]. Based on the eigenvalue analysis of the moment tensor, a generalized treatment for the classification of crack type and the determination of crack orientation is implemented as the SiGMA (simplified Green's functions for moment tensor analysis) code[4]. The procedure has been successfully applied to fracture tests of concrete[5],[6],[7]. Elsewhere, a similar procedure was reported[8] but limited to the two-dimensional (2-D) problem, for which the SiGMA-2D code is available[9].

In order to apply fracture mechanics to fracture modes of concrete structures, the nucleation of the fracture process zone ahead of the crack tip has been intensively studied[10]. Fracture mechanics recently covers the continuous damage mechanics[11]. In the present paper, a relation between the damage variables and the moment tensor components is clarified. In bending tests of notched beams, crack kinematics and the damage evolution in the fracture process zone are estimated by the moment tensor analysis of the SiGMA.

2. MOMENT TENSOR AND DAMAGE VARIABLES

Mathematically crack kinematics can be modeled by the crack motion vector $\mathbf{b}(\mathbf{y},t)$ and

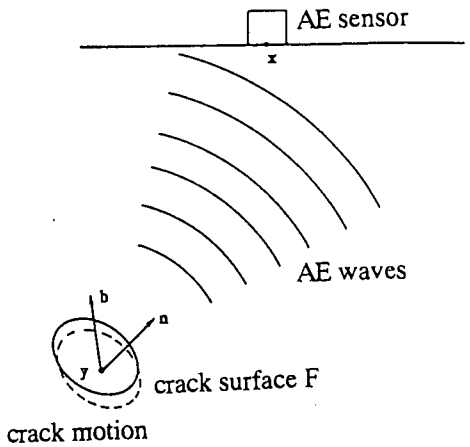

Fig. 1 Crack nucleation and AE waves.

the unit vector **n** normal to the crack surface F as shown in **Fig. 1**. The vector **b**(**y**,t) is referred to as b(**y**)**l**S(t), where b(**y**) represents the magnitude of crack displacement, **l** is the direction vector of crack motion, and S(t) is the source-time function of crack nucleation. The following integration over the crack surface F leads to a product of the moment tensor m_{pq} and the source-time function S(t):

$$\begin{aligned} &\int_F C_{pqkl}\,[b(\mathbf{y})l_k S(t)]\,n_l\,dS \\ &= [C_{pqkl}l_k n_l]\,[\int_F b(\mathbf{y})\,dS]S(t) \\ &= [C_{pqkl}l_k n_l]\,\Delta V\,S(t) = m_{pq}\,S(t), \end{aligned} \quad (1)$$

where C_{pqkl} is the tensor of elastic constants and ΔV is the crack volume.

The elastic displacement $\mathbf{u}(\mathbf{x},t)$ due to the crack motion $\mathbf{b}(\mathbf{y},t)$ represents AE wave[3],

$$u_i(\mathbf{x},t) = G_{ip,q}(\mathbf{x},\mathbf{y},t)\,m_{pq} * S(t). \quad (2)$$

Here $G_{ip,q}(\mathbf{x},\mathbf{y},t)$ is the spatial derivatives of Green's functions and the symbol $*$ denotes the convolution operation.

In an isotropic material, the moment tensor m_{pq} is derived from eq. (1),

$$\begin{aligned} m_{pq} &= [C_{pqkl}\,l_k n_l\,]\,\Delta V \\ &= [\lambda l_k n_k + \mu l_p n_q + \mu l_q n_p]\Delta V, \end{aligned} \quad (3)$$

where λ and μ are Lame constants. A product of the crack vector $b(\mathbf{y})l_k$ and the crack normal n_l is referred to as the eigenstrain in the micromechanics [12]. Similarly, in the damage mechanics, the second-order damage tensor εP_{kl} is defined[13] as,

$$\varepsilon P_{kl} = 1/V^* \sum_i \Delta F\,(b_k n_l + b_l n_k)^{(i)}/2, \quad (4)$$

where V^* is the representative volume and ΔF is the area of one crack. Taking into account only one crack, the damage tensor $\varepsilon 1_{kl}$ for one crack is derived from eq. (4),

$$\begin{aligned} \varepsilon 1_{kl} &= 1/V^* \int_F ([b(\mathbf{y})l_k]\,n_l + [b(\mathbf{y})l_l]\,n_k)\,dS/2 \\ &= \Delta V\,(l_k n_l + l_l n_k)/2V^*. \end{aligned} \quad (5)$$

The scalar damage variable for one crack D is readily obtained as,

$$D = n_k\,\varepsilon 1_{kl}\,n_l = \Delta V/V^*\,l_k n_k. \quad (6)$$

From eq. (3), the trace component is obtained,

$$m_{kk} = (3\lambda+2\mu)\,l_k n_k \Delta V. \quad (7)$$

Consequently, the damage evolution can be represented as,

$$\begin{aligned} \sum D^{(i)} &= 1/V^* \sum_i [\Delta V\,l_k n_k]^{(i)} \\ &= 1/[V^*\,(3\lambda+2\mu)] \sum_i m_{kk}^{(i)}. \end{aligned} \quad (8)$$

This implies that the damage evolution process is estimated relatively from the accumulation of the trace components of the moment tensors. Also, the relative crack volume can be obtained from eq. (7) as,

$$(3\lambda+2\mu)\,\Delta V = m_{kk}/[l_k n_k]. \quad (9)$$

3. SiGMA PROCEDURE

In the SiGMA code, eq. (2) is simplified, taking into only the amplitude of the first motion A(**x**) of AE wave in the far field,

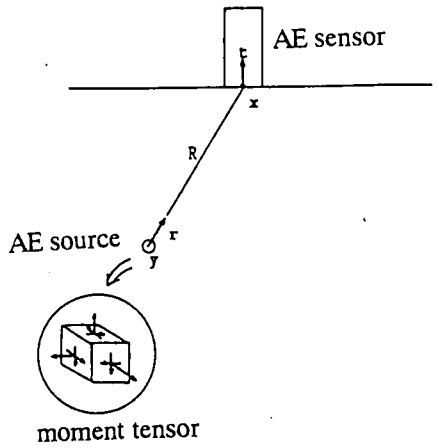

Fig. 2 Configuration of AE sensor and AE source.

$$A(x) = Cs / R \; Ref(\mathbf{t},\mathbf{r}) \; r_p \; m_{pq} \; r_q, \qquad (10)$$

where Cs is the calibration coefficient. As shown in **Fig. 2**, **t** is the direction of the sensor sensitivity. R is the distance from AE source at point **y** to AE sensor at point **x**. r_p is its direction vector. Ref(**t**,**r**) is the reflection coefficient. Since the moment tensor is symmetric and of the second order, the number of independent unknowns m_{pq} is six. A multi-channel observation of the first motions at more than six sensor locations can provide sufficient information to solve eq. (10).

Prior to the analysis, calibration coefficient Cs in eq. (10) should be determined to compensate the sensitivity of AE sensors. Then three eigenvalues are normalized and uniquely decomposed into three ratios X, Y, and Z[4],

$$\begin{aligned} &1.0 = X + Y + Z, \\ &\text{the intermediate eigenvalue/the maximum} \\ &\quad = 0 - Y/2 + Z, \qquad (11) \\ &\text{the minimum eigenvalue/the maximum} \\ &\quad = -X - Y/2 + Z, \end{aligned}$$

where X, Y, and Z denote the shear ratio, the deviatoric tensile ratio, and the isotropic tensile ratio, respectively. AE sources for which the shear ratios X are smaller than 40% are classified as tensile cracks. AE sources of the shear ratio X greater than 60% are referred to as shear cracks. In the case between 40% and 60%, AE sources are classified as mixed-mode.

Table 1 Mixture proportions

	weight per unit mass (kg/m³)				(cc)	(cm)	(%)
	W	C	S	G	AE admix-ture	slump	air
concrete	172	346	834	1021	104	8.0	5.0
mortar	342	570	1140	-	-	-	-

In the SiGMA code, unit vectors $\mathbf{e}_1$, $\mathbf{e}_2$ and $\mathbf{e}_3$ corresponding to three eigenvectors **l** + **n**, **l** x **n** and **l** - **n** are determined. Therefore, the vectors **l** and **n** can be recovered from the following relations,

$$\begin{aligned} \mathbf{l} &= (2 + 2l_k n_k)^{1/2}\mathbf{e}_1 + (2 - 2l_k n_k)^{1/2}\mathbf{e}_3, \\ \mathbf{n} &= (2 + 2l_k n_k)^{1/2}\mathbf{e}_1 - (2 - 2l_k n_k)^{1/2}\mathbf{e}_3. \end{aligned} \qquad (12)$$

4. EXPERIMENTS

(1) Bending Tests

The flaw location procedure was successfully applied to identify the fracture process zone in concrete[14]. Because the SiGMA procedure provides information on crack types and crack orientation, in addition to crack location, crack nucleation in the fracture process zone is investigated.

Mortar and concrete specimens of dimensions 10 cm x 10 cm x 40 cm were cast and cured in water for 28 days in the standard room (20°C). These mixture proportions are given in **Table 1**. The maximum size of coarse aggregate is 20 mm, and fine aggregate is common in both mixes of concrete and mortar. Mechanical properties are indicated in **Table 2**. These were determined from cylindrical specimens of 10 cm diameter and 20 cm height at the age of 28 days. Although the strength of mortar is comparable to that of concrete, Young's modulus and P-wave velocity of mortar are even lower than those of concrete.

Tests of three-point bending were conducted. At the age of 28 days, sawed pre-cracked notch of 3 cm depth and 1 mm width was introduced in each specimen. The types of specimens include a center-notched beam under center

Table 2 Mechanical properties

	compressive strength (MPa)	tensile strength (MPa)	Poisson's Ratio	Young's modulus (GPa)	P-wave velocity (m/s)
concrete	52.8	4.12	0.24	32.5	4730
mortar	53.7	2.93	0.20	23.4	4130

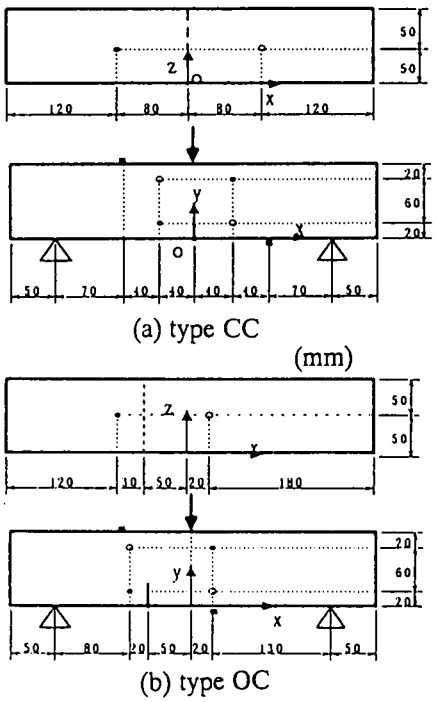

Fig. 3 Experimental set-up and AE sensor array.

loading (type CC), and an off-center notched beam under center loading (type OC). The experimental set-ups and AE sensor locations are shown in **Fig. 3**. Six AE sensors are arranged to cover the area of the fracture process zone to be nucleated. In the figures, open circles indicate AE sensors located at the back face and solid circles are those on the top face. All sensors are of the resonant frequency 150 kHz. These are relatively calibrated in order to obtain equivalent sensitivities beforhand. The frequency range from 10 kHz - 1 MHz and total 60 dB gain for amplification are employed.

AE waveforms under crack extension were detected, amplified, filtered and recorded by using the LOCAN-TRA system (Physical Acoustics Corp.). Loads were measured by a load-cell and the crack-mouth opening displacements (CMOD) were recorded by a clip gauge inserted into the notch. A servo-valve controlled machine was employed for loading.

Specimens of the type CC were prepared to trace the nucleation of the fracture process zone under mode-I cracking. In contrast, the mixed-mode of mode-I and mode-II cracking was expected in the type OC. The loading speed of 0.01 mm/min was applied to the type CC specimens, whereas the loading speed applied to the type OC specimens was 0.02 mm/min. This is because crack propagation of the type CC was faster than that of the type OC.

(2) Waveform Analysis

In order to solve eq. (10), the amplitude of the first motion should be read from AE waveform. In addition, the arrival time of the first motion need be determined to carry out the location analysis. These two parameters of the arrival time and the amplitude of the first motion were read visually, by displaying each waveform on the CRT screen. From AE waveforms at six locations, the locations and moment tensor components were determined. The crack types and the crack orientations were then analyzed.

In order to estimate errors of the moment tensors, an error analysis was performed assuming location errors[4]. Then, it was realized that the accuracy was highly dependent on the geometrical configuration between the sensor array and AE sources. It implies that the accuracy of the solutions is dependent on the cases and may not be able to be estimated by the simple criterion. Furthermore, it is found that most error could be introduced from misreading of the first motions. To select reliable solutions, therefore, a post-analysis was developed[15]. Theoretical AE waveforms at AE sensor locations were synthesized, by using the data of AE source location and the moment tensor components. The two parameters of each theoretical waveform were automatically read and the SiGMA code was applied again. Then, AE sources of which crack kinematics in the post analysis were in good agreement with those of the SiGMA analysis were selected as reliable solutions.

Table 3 The number of AE hits analyzed

		total AE hits	clear records	SiGMA analyzed	post-analysis
concrete	type CC	205	177	137	36
	type OC	515	212	143	29
mortar	type CC	254	207	147	43
	type OC	975	609	409	102

5. RESULTS AND DISCUSSION

The numbers of total AE hits detected in the tests are indicated in **Table 3**. AE hit is defined as one AE event for which AE waveforms are simultaneously recorded at all channels. From the data of AE hits, however, all the first motions could not be necessarily identified. The AE hits of which the first motions were clearly recorded at all six channels were selected for the analysis. The number of these data is denoted in the table. In the case of the type OC of concrete, more than 50% of AE hits are discarded. After the SiGMA analysis, as a result, approximately half of the total AE hits could have solutions except for the type OC of concrete. Eventually, by the post-analysis, the numbers of the data further decrease up to 10 - 20 % of the total. This is the limitation of the feasibility of the SiGMA analysis at the current state. AE events discarded in the analysis mostly result from unclear first motions and divergence in the location routine. The situation might be improved by introducing automated first-motion reading[8].

In contrast to AE hits, AE counts are defined as the number of AE occurrence which is recorded at one channel. In **Fig. 4**, AE counts observed at AE sensor of channel 1 are plotted against CMOD, along with the load-displ acement curve. The type CC of concrete in **Fig. 4** (a) shows a typical result. After the peak load, AE activity suddenly increases and thus the discontinuous jumps of AE occurrence are observed. In the type OC of concrete, a similar activity was found. It suggests that the cracking process in concrete is not successive. As shown in **Fig. 4** (b), in the case of type OC of mortar, AE activity increases gradually

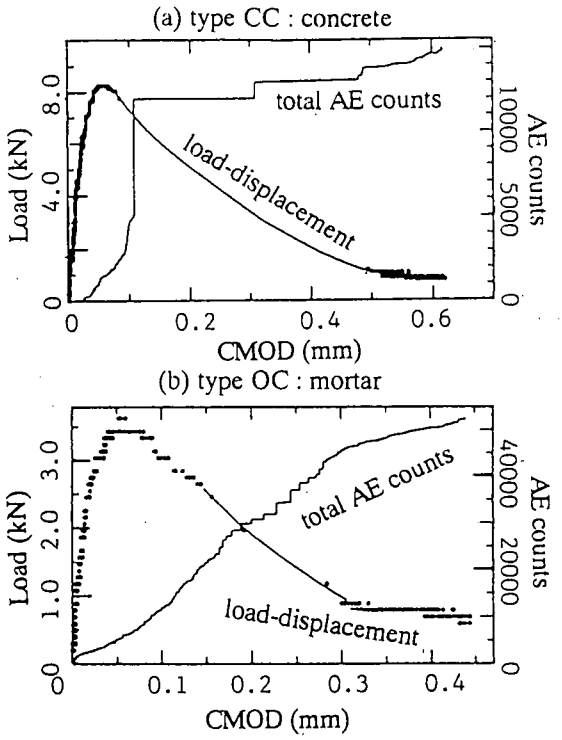

Fig. 4 Load-CMOD relations and total AE counts observed under loading.

with no relation to the peak load. Although a slight increase of AE activity was found at the peak load in the type CC of mortar, an essential behavior of AE occurrence is similar to **Fig. 4** (b). This implies that microcracks in the fracture process zone are generated continuously in mortar.

Results of the post-analysis are plotted in **Figs. 5** and **6**. AE sources for which the shear ratios are smaller than 40 % and classified tensile cracks are indicated by "arrow" symbol, while other sources are indicated by "cross" symbol.

AE sources are plotted at their locations with directing the two vectors, which are determined from eq. (12). Previously, only the first eigenvectors $\mathbf{e}_1$ was plotted for the tensile cracks[4]. Recent study, however, clarifies that the angle between the two vectors **l** and **n** could be over 50° in even the case that the shear ratio is smaller than 40%[16]. Consequently, the directions of the two vectors are given for all the data. As matter of course, the angles between the two directions are con-

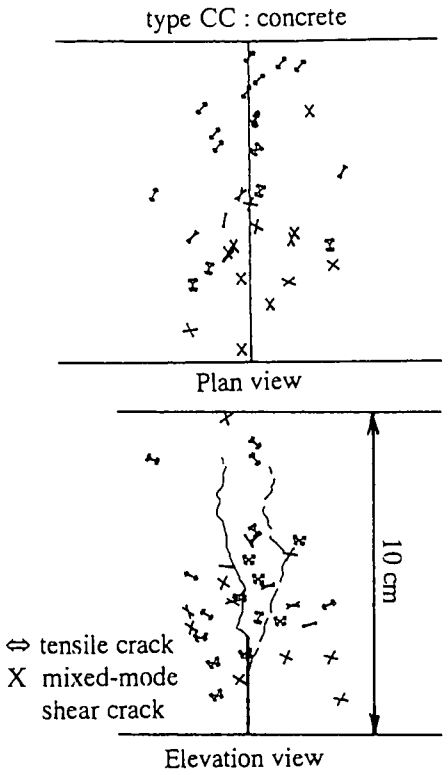

Fig. 5 Crack locations, types and orientations determined in the type CC of concrete.

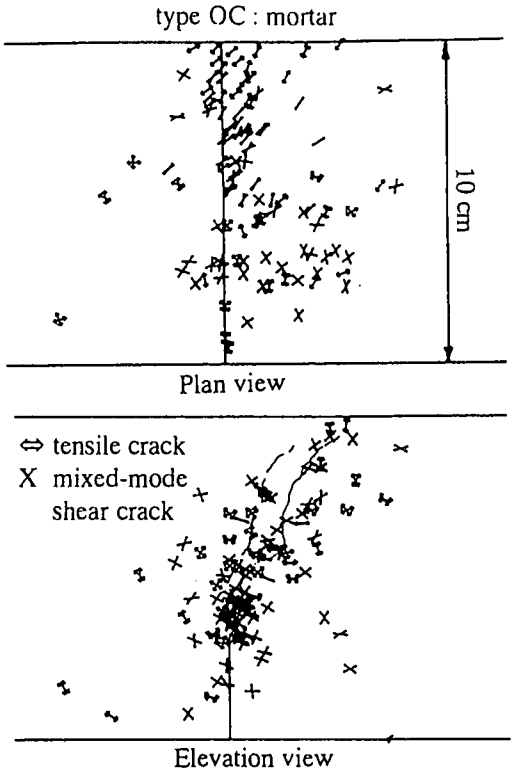

Fig. 6 Crack locations, types and orientations determined in the type OC of mortar.

siderably small for the tensile cracks with the "arrow" symbol.

In **Fig. 5**, a result of the CC type specimen of concrete is given. Surface cracks extended from the notch are indicated in the elevation view. These were observed at the top face and the back face. The final crack surface is created tortuously to the notch, and thus the directions of the tensile opening are inclined to the notch according to the plan view. It seems that AE cluster covers the fracture process zone and tensile cracks are observed at the outer region of the zone.

In **Fig. 6**, a result of the type OC of mortar is shown. Surface cracks are created diagonally from the notch to the loading point. Thus, mixed-mode crack propagation is observed. Along the final crack surface, intense AE cluster is found. Under mixed-mode cracking, a wide region corresponding to the fracture process zone is observed. Again, tensile cracks are mainly observed far from the surface cracks and the cluster of shear cracks.

To confirm the tendency of AE locations, AE sources were projected on the x-y plane in **Fig. 3**. The case of the type OC specimen of concrete is shown in **Fig. 7**. Cracks are classified into tensile, mixed-mode, and shear cracks. Locations of the surface cracks are denoted by open circles. The final crack extends from the left to the right. Most of tensile cracks are observed farther from the surface cracks than mixed-mode and shear cracks which are observed close to the surface cracks. Similar results were also obtained in the other cases. This demonstrates that the tensile cracks are nucleated at the outer region of the fracture process zone, while the other-type cracks are generated intensely inside the process zone.

Damage evolution was estimated by eq. (8). The accumulation of crack volume was also estimated from eq. (9). In **Fig. 8**, results of the type CC of concrete and the type OC of mortar are plotted. From the experimental dat a, the trace of the moment tensor was directly calculated. As a result, both the scalar damage

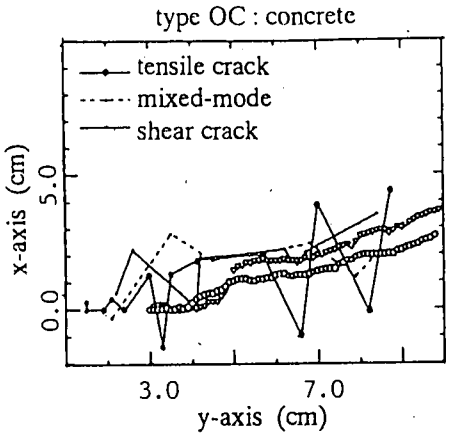

Fig. 7 Projection of AE locations in the type OC of concrete.

m_{kk} and the variable $m_{kk}/l_k n_k$ corresponding to the crack volume are relative. The accumulating process of these values is plotted against the number of AE hits. Although cracks are classified, three types of cracks are generated so mixed-up that the dominant type can not be identified in the accumulation process. As seen in **Fig. 8** (a), the damage evolution and the accumulation of crack volume are discontinuously step-up. According to **Fig. 8** (b), the damage evolution in mortar is fairly continuous although a slight step-like increase is observed in the accumulation of crack volume.

Taking into account the difference of AE activities in **Fig. 4**, the discrepancy of the damage evolution could result from the presence of coarse aggregate. The step-like increases of the damage and the crack volume possibly correspond to the bonding failure between coarse aggregate and mortar matrix.

In the type CC specimens, mode I cracking was expected, while mixed-mode cracking was suggested in the type OC. The discrepancy, however, of the damage evolution process was not clear in concrete. The evolution process was always step-like discontinuous. On the other hand, the damage evolution of mortar was observed to be successive under the nucleation of the fracture process zone. This implies that the damage evolution in the fracture process zone of cementitious materials is not necessarily dependent on the mode of final cracks, but responsible for the nucleation of microcracking.

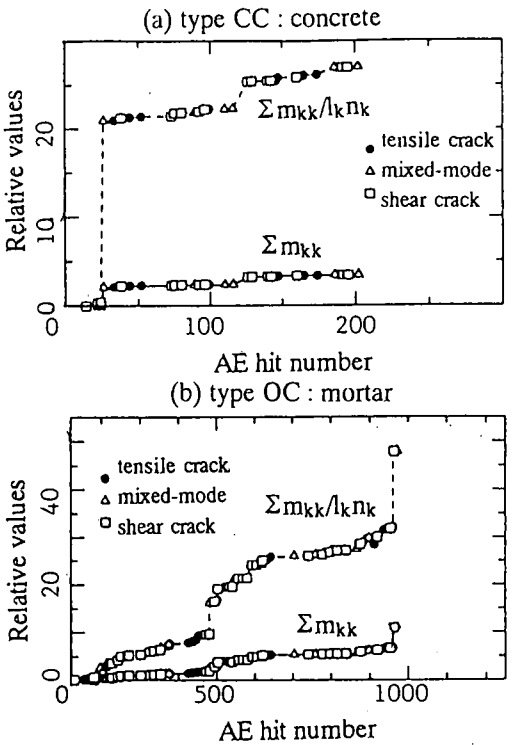

Fig. 8 Damage evolution and the accumulation of crack volume.

6. CONCLUSION

Applying the moment tensor analysis of AE, the damage evolution process under the nucleation of the fracture process zone is estimated in concrete and mortar. Conclusions obtained are as follow:

(1) Although specimens for mode-I cracking and for mixed-mode cracking are prepared, the cracking processes (AE generations) of the both cases are observed to be not successive in concrete. In contrast, microcracks in the fracture process zone are generated continuously in mortar.

(2) From the SiGMA analysis, it is found that tensile cracks are observed farther from the surface cracks than mixed-mode and shear cracks. This demonstrates that the tensile cracks are nucleated at the outer region of the fracture process zone, while the shear cracks are generated inside the zone and close to the final crack surface.

(3) In concrete, the damage evolution in the fracture process zone is step-like discontinuous, while that of mortar is considerably successive. The discrepancy between

the mode-I cracking and the mixed-mode cracking in the damage evolution process is not clear. This implies that the damage evolution in cementitious materials is not necessarily dependent on the mode of final cracks, but associated substantially with the nucleating mechanisms of microcracking.

REFERENCES

1) Ohtsu, M.: Source Mechanism and Waveform Analysis of Acoustic Emission in Concrete, Journal of AE, Vol. 2, No. 1, 103 - 112, 1982.
2) Wadley, H. N. G. and Scruby, C. B. : Acoustic Emission Source Characterization, *Advances in Acoustic Emission*, Dunhart Publishers, Knoxville, 125-153, 1981.
3) Ohtsu, M.:Mathematical Theory of Acoustic Emission and Moment Tensor Solution, Journal of the Society of Materials Science, Japan, Vol. 36, No. 408, 1025-1031, 1987.
4) Ohtsu, M.:Simplified Moment Tensor Analysis and Unified Decomposition of AE Source, Journal of Geophysical Research, Vol. 96, No. B4, 6211-6221, 1991.
5) Ohtsu, M., Shigeishi, M. and Iwase, H.: AE Observation in the Pull-Out Process of Shallow Hook Anchors, Proc. JSCE, No. 408/V-11, 177-186, 1989.
6) Suaris, W., van Mier, J. G. M.:Acoustic Emission Source Characterization in Concrete under Biaxial Loading, Materials and Structures, No. 28, 444-449, 1995.
7) Yuyama, S., Okamoto, T., Shigeishi M. and Ohtsu, M.:Acoustic Emission Generated in Corners of Reinforced Concrete Rigid Frame under Cyclic Loading, Materials Evaluation, Vol. 53, No. 3, 409-412, 1995.
8) Ouyang, C., Landis, E. and Shah, S. P.: Damage Assessment in Concrete using Quantitative Acoustic Emission, Journal of Engineering Mechanics, ASCE, Vol. 117, No. 11, 2681-2698, 1991.
9) Shigeishi, M. and Ohtsu, M.: Acoustic Emission Waveform Analysis in Two-Dimensional Models, Journal of the Society of Materials Science, Japan, Vol. 45, No. 9, 1055-1060, 1996.
10) Mihashi, H.:State-of-the-Art Report on Fracture Mechanics Applied to Reinforced Concrete Structures, Concrete Journal, JCI, Vol. 34, No. 5, 5-15, 1996.
11) Shah, S. P., Swartz, S. and Ouyang, C. S.: *Fracture Mechanics of Concrete*, John Wiley & Sons, Inc., New York, 1995
12) Mura, T.: *Micromechanics of Defects in Solids*, Martinus Nijhoff Publishers, The Hague, 1982.
13) Kachanov, M.:Effective Elastic Properties of Cracked Solids : Critical Review of Some Basic Concepts, Applied Mechanics Reviews, Vol. 45, No. 8, 304-335, 1992.
14) Nomura, N., Mihashi, H. and Niiseki, S.: Influence of Coarse Aggregate Size on Fracture Energy and Tension Softening of Concrete, Concrete Research and Technology, JCI, Vol. 2, No. 1, 57-66, 1991.
15) Ohtsu, M.: Post-Analysis of SiGMA Code for Acoustic Emission Moment Tensor Analysis, Journal of JSNDI, Vol. 43, No. 12, 776-782, 1994.
16) Ohtsu, M.: Acoustic Emission Theory for Moment Tensor Analysis, Research on Nondestructive Evaluation, No. 6, 169-184, 1995.

(Received August 22, 1997)

AE法によるコンクリートの破壊進行領域における損傷過程の考察

大津　政康・大塚　政暢

AE波形のモーメントテンソル解析法により，AE発生源の機構の同定が可能となっている．そこでノッチ付き供試体の曲げ試験を行い，ノッチ先端の破壊進行領域の形成過程の解明に適用した．モーメントテンソル成分と損傷力学パラメータの関係についても検討し，モーメントテンソルから損傷過程の評価も試みた．破壊進行領域の形成過程では，いずれの供試体でもAE源はある範囲に広く発生し，引張クラックがその外縁部に，せん断クラックが最終破壊面近傍に主に観察された．一方，損傷過程については，コンクリートではステップ状に不連続的に累積され，モルタルでは漸増的に累積されることが認められ，破壊進行領域での損傷累積には，破壊モードより微小クラックの発生過程に依存することが明らかになった．